Vacuum enclosures for solar thermal panels Part 2: Transient testing with an uncooled absorber plate

Farid Arya[a*], Roger Moss[b], Trevor Hyde[a], Stan Shire[b], Paul Henshall[c], Philip Eames[d]

[a] *Centre for Sustainable Technologies, Ulster University, UK*
[b] *School of Engineering, University of Warwick, UK*
[c] *School of Architecture, Oxford Brookes University, UK*
[d] *Centre for Renewable Energy Systems Technology, Loughborough University, UK*
[*]*Corresponding Author*

Email: f.arya@ulster.ac.uk; r.moss@warwick.ac.uk; t.hyde@ulster.ac.uk; stan.shire@warwick.ac.uk; phenshall@brookes.ac.uk; p.c.eames@lboro.ac.uk.

Abstract

Creating a vacuum (<1Pa) around a solar absorber in a flat plate solar thermal collector can increase efficiency by minimising gaseous conduction and convection between the absorber plate and the glass cover. High performance and architecturally attractive flat plate solar thermal collectors are appealing to building owners and designers for supplying clean and renewable energy cost effectively produced via the façade of the building.

This two part paper describes the construction techniques and thermal performance of two vacuum enclosures, fabricated at Ulster University, as prototype components for evacuated flat plate solar collectors. The enclosures were tested at three conditions: 0.0033 Pa, 17 Pa and atmospheric pressure. The first enclosure consisted of two glass panes, sealed to an edge spacer and separated by an array of support pillars on a regular square grid to form a narrow evacuated space. The second enclosure, incorporated an uncooled copper plate to represent a solar thermal absorber. Part 1 of this paper has described the fabrication techniques and compared results from hot-box calorimeter and IR thermography testing of the first enclosure with numerical and analytical predictions.

Part 2 describes solar simulator testing of the second enclosure which incorporated an uncooled copper plate. Testing under a solar simulator showed a higher stagnation temperature in the high vacuum test (0.0033 Pa) in comparison with the low vacuum (17 Pa) and atmospheric pressure tests. Curve fitting of a heat transfer model to the transient response data demonstrated that radiation and gas conduction were close to predictions. Simulated results were in close agreement with both the transient response and the steady-state asymptotic plate temperatures.

Keywords: solar absorber; evacuated flat plate solar collector; transient heat transfer.

1. Introduction

The experimental analysis reported in this paper (Part 2) was designed to investigate the ability of a prototype pillar-supported evacuated enclosure to reduce heat losses from a thermal absorber plate. The success of the enclosure design in safely withstanding atmospheric pressure loading under high vacuum conditions has been reported elsewhere (Part 1 of this paper) which demonstrates its suitability for flat plate solar thermal collectors. When constructed as a flat plate solar thermal collector, this design is architecturally appealing as it can be integrated directly into a building façade where it would combine the functionality of vacuum insulation, solar shading and solar heat collection in a single component.

An evacuated enclosure was fabricated which incorporated an uncooled copper plate i.e. it was isolated inside the vacuum enclosure. The plate temperature was recorded in a transient experiment as a measure of the instantaneous heat flux over a wide range of plate temperatures including 25°C - 121°C, 25°C - 104°C and 25°C - 103°C for the internal pressures of 0.0033 Pa, 17 Pa and atmospheric, respectively. This experimental technique mimics the behaviour of a water-cooled absorber but with greatly reduced complexity in terms of fabrication and instrumentation.

As there is no thermal fluid the absorber cannot be held at a constant temperature and there is no heat extracted; therefore the system does not have a collector efficiency. However, we can infer an equivalent efficiency indirectly from the transient response: this is an estimate of the efficiency that would be possible if the enclosure were used in an evacuated solar thermal collector.

Test procedures for conventional collectors that take account of transient effects to improve the accuracy of quasi-steady efficiency measurements have been reviewed by Amer et al. (1997); an improved method is described by Amer and Nayak (1999). Rodríguez-Hidalgo et al. (2011a, b) performed an outdoor experimental study of the transient behaviour of a conventional water-cooled flat panel. The experiment described in this study is however completely transient. Three types of analysis have been performed:

- A curve fit to the transient response. This estimates the plate absorbance, emissivity and gas conductivity.
- A prediction of the steady state glass cover temperature for any given plate temperature based upon heat transfer by natural convection, radiation and conduction.
- An estimate of the time constants for plate, glass and the overall system.

2. Nomenclature

c	Specific heat capacity		Nu	Nusselt number
d	Gap between plate and glass		Pr	Prandtl number
h	Surface heat transfer coefficient		Ra	Rayleigh number
k	Conductivity		T	Temperature (K)
p	Pressure		U_L	Overall heat loss coefficient
$p_{1,2,3}$	Curve fit coefficients		W	Width of plate
$\dot{q}$	Heat flux (W/m^2)		α	Absorbance
t	Time		ε	Emissivity
w	Area density (kg/m^2)		η	Efficiency
D	Pillar diameter		ρ	Reflectance
G	Insolation from solar simulator (W/m^2)		σ	Stefan-Boltzmann constant
H	Height of plate		τ	Transmissivity
L	Characteristic length for Nusselt and Raleigh numbers			

3. Experimental Study of Enclosure with Integrated Copper Plate

Following the detailed analysis of an empty vacuum enclosure in part 1 of this paper, a vacuum enclosure was fabricated incorporating a copper plate to mimic a solar absorber, (Figure 1), to study the high temperature capability of evacuated flat plate collectors via a transient heating and cooling investigation.

3.1 Fabrication of Vacuum Enclosure and Absorber

A C101-grade copper plate was polished and painted with Solkote® solar panel paint using a spray gun. A number of thin coats were applied to ensure a uniformly coated surface was achieved. The emissivity of the copper sheet was measured prior to assembly using an emissometer (Devices and Services Co. model: AE1-2197). The top and bottom surface of the copper plate had emissivities of 0.64 and 0.5 respectively; the difference in these emissivities was due to the manual application of the coatings. Lower emissivities might have been possible with a thinner coating; this would however have adversely reduced the absorbance of the plate. After painting, the copper plate was baked at 200°C for 2 hours to enable the volatile components of the coating to evaporate thus minimising future contamination of the vacuum enclosure. Commercially available solar absorbers use highly optimised selective absorbance coatings with very low infrared (IR) emissivities to reduce heat loss, however these could not be procured for a one-off absorber. The relatively higher emissivity of the Solkote used in this experiment did not detract from the estimation of gas conduction losses.

The copper absorber plate was supported 8 mm above the bottom glass pane by four glass pillars (Figure 1a) which were fixed to both the copper plate and the bottom glass pane using the proprietary adhesive Araldite (Araldite, 2011). Although outgassing from the adhesive has the potential to raise the vacuum pressure, previous experience suggested the small quantity required would have little effect on the vacuum stability over a 3 day test period in this study. These support pillars were the only contact points between the absorber and the vacuum enclosure with a gap of 6.3 mm between the copper plate and the top glass cover of the enclosure. The copper plate was 360 × 360 mm, 0.9 mm thick, with 10.5 mm diameter holes at a 50 mm pitch to accommodate the support pillars.
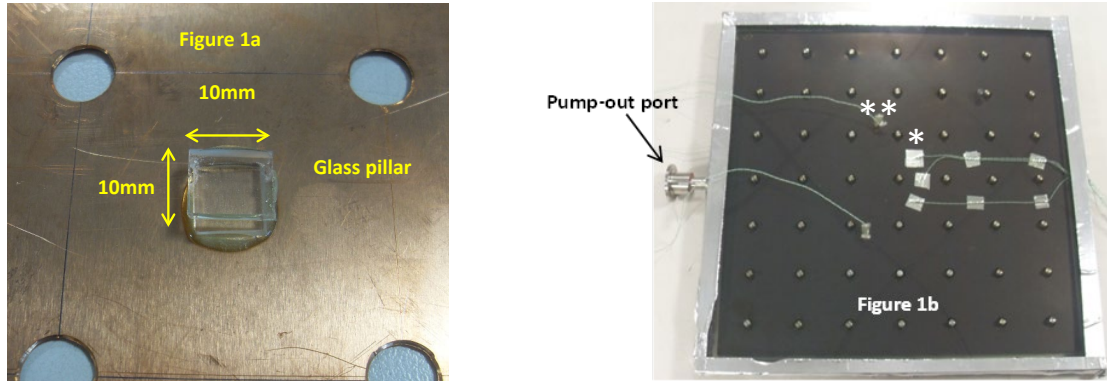
Figure 1(a). Copper plate and glass pillar prior to spraying with Solkote®, (b) Copper plate mounted in the vacuum enclosure showing thermocouple positions and vacuum pump-out port.

A series of thermocouples were attached to each side of the absorber and two thermocouples were attached to each glass cover pane as shown in Figure 1(b). During solar simulator test the thermocouple readings across each surface were almost identical. The readings from thermocouple location "*" for the copper plate and "**" for the top glass are used in this work. The thermocouple wires exited the enclosure through a port in the stainless steel edge spacer. These thermocouples were covered with a highly reflective aluminium foil tape to minimize the impact of direct illumination during this investigation which might result in higher temperature readings.

During solar simulator testing the temperature difference between the top and bottom enclosure glass panes was minimal, therefore conduction along the support pillars was not expected to produce local hot/cold spots (as seen in hot box testing) that might influence thermocouple readings.

The separating support pillars for the glass panes were carefully positioned to avoid contact between the pillars and the copper plate. The fabrication procedure for the enclosure was similar to that described previously (Part 1 of this paper). With the previous enclosure the low-emissivity coatings of each glass cover pane faced inwards to the cavity, as is conventional in insulating glazing units. As this enclosure was intended for testing under more severe conditions the low emissivity coatings faced outwards in an attempt to guarantee the strongest possible bond between solder and glass for sealing the edge of the enclosure.

3.2 Solar Simulator

The solar simulator, shown in Figure 2, has an array of 35, 1200W OSRAM HMI lamps with a zoom optical system and uniform focusing, a cooling fan and iris diaphragm. These lamps are AC-operated discharge lamps in which the luminous arc burns in a dense vapour atmosphere comprising mercury and rare earth halides; the spectrum is similar to the AM 1.5 standard solar spectrum. The illuminated region is 1.8m by 2.6m therefore the illumination is expected to be uniform over the absorber area of 0.36 × 0.36 m.
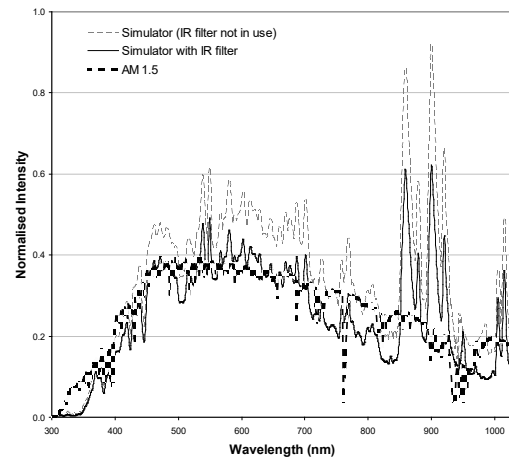

Figure 2. Solar simulator and measured spectral distribution of the solar simulator compared to the standard AM 1.5 reference spectrum (Pugsley et al., 2017; Arya, 2014).

3.3 Solar Simulator Test

The enclosure was connected to a vacuum pump via a 10 mm internal diameter pump-out port through the stainless steel edge spacer. In this test the pump-out port was not sealed and the vacuum pump operated throughout the solar testing. The enclosure was placed under the solar simulator and evacuated until the vacuum pressure stabilised. The enclosure was covered with 150 mm thick Styrofoam, the simulator was activated for 15 minutes to reach a constant output; then the foam was removed to illuminate the enclosure. The enclosure was positioned horizontally and supported at its four corners so that air could circulate freely underneath. The simulator lamp array was set parallel to the plate i.e. pointing vertically downwards at a height of 1.8 m above the enclosure to provide uniform illumination and avoid hot-spots from the beam of each lamp.

To determine the effect of vacuum pressure on heat loss from the copper absorber plate the vacuum enclosure was tested while under high vacuum (0.0033 Pa), medium vacuum (17 Pa) and no vacuum. Each test commenced by illuminating the enclosure at a constant simulator power until the plate temperature stabilised. The simulator was then switched off and data recording continued until the plate temperature was close to ambient. The data sampling rate was 0.1 Hz.

3.4 Solar Simulator Experimental Results

In the first experiment the solar simulator was activated for 5 hours while a high vacuum (0.0033 Pa) was maintained in the enclosure using a turbo molecular vacuum pump (Edwards T-Station). After 5 hours the copper absorber plate temperature had reached 121.8°C and was approaching steady state conditions. The solar simulator was switched off to allow the copper absorber to cool down; taking 2 hours and 13 minutes for the absorber temperature to reach 25°C. In the second experiment a medium vacuum (17 Pa) was maintained in the enclosure using a Leybold rotary pump. After 2 hours and 35 minutes the copper absorber temperature had stabilised at 104.2°C. At this point the solar simulator was switched off to allow the copper absorber to cool down; taking 2 hours and 10 minutes for the absorber temperature to reach 25°C. In the third experiment, the enclosure was not evacuated and was open to atmosphere to prevent any pressure rise due to an increase in air temperature inside the enclosure. After 1 hour and 40 minutes the copper absorber temperature had stabilised at 103.6°C. The solar simulator was switched off to allow the copper absorber to cool down; taking 1 hour 52 minutes to reach 25°C. The heating and cooling profiles for the three tests are compared in Figure 3 and Table 1; for ease of interpretation, the upper graph is at the highest pressure despite being last chronologically.
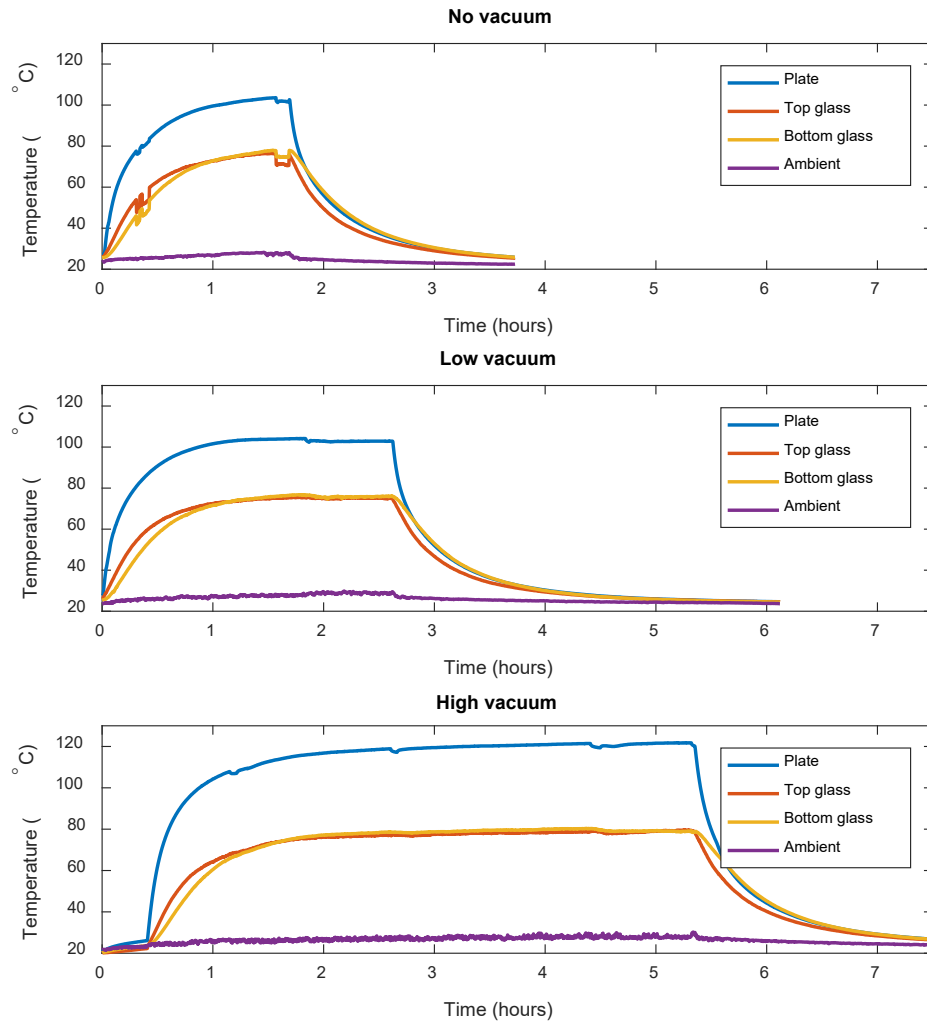
Figure 3. Comparison of the heating and cooling profiles during solar simulator testing.

Table 1. Comparison of peak temperatures and cooling times for copper plate in the vacuum enclosure. The steady-state prediction assumes a uniform glass temperature (see below)

Vacuum pressure	Maximum plate temperature	Predicted steady-state plate temperature	Cooling time to 25°C
No vacuum	103.6°C	106.0°C	112 minutes
17 Pa	104.2°C	106.1°C	130 minutes
0.0033 Pa	121.8°C	118.6°C	133 minutes

The turbo-molecular vacuum pump continued to operate throughout the high vacuum test. Under solar illumination, the temperature of the copper absorber and glass panes increased and outgassing occurred. The outgassing rate initially caused the pressure to increase; however after 1 hour the outgassing fell below the pumping rate and the pressure returned to the pre-illumination level as illustrated in Figure 4. The vacuum pressure was measured using a vacuum gauge (Leybold: PTR 90 PENNINGVAC) which was connected to the pump-out port of the enclosure via a Tee-connection.
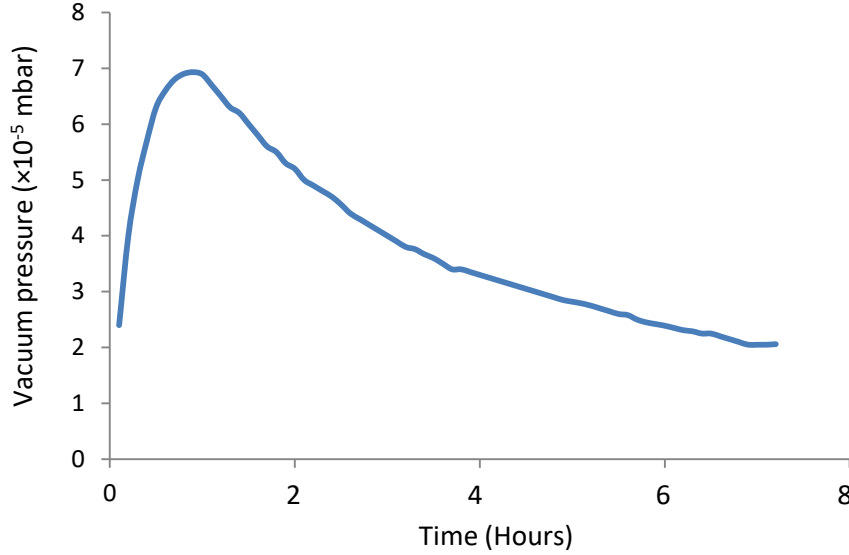
Figure 4. Vacuum pressure increase due to outgassing of the copper absorber and internal glass surfaces.

The low vacuum test used a rotary pump to achieve an ultimate pressure of 17 Pa. When the solar simulator was activated the vacuum pressure appeared to remain stable (a Leybold TR-211 PIRANI gauge was used to measure the vacuum pressure). This may indicate that the outgassing experienced during the first test had removed a large part of the absorbed gases, however it is more likely that the pressure rise as seen in the first test would simply be indistinguishable at the low vacuum pressure of 17 Pa.

3.5 Discussion of Solar Simulator Test Results

The copper absorber plate reached a similar ultimate temperature (approximately 104°C) in both the low vacuum and atmospheric tests, suggesting that the pressure of 17 Pa was insufficient to significantly change the gaseous conduction. However, in the high vacuum test, the copper absorber plate reached a temperature of 122.4°C indicating that gaseous conduction had been supressed. In each case, the plate reaches an equilibrium or stagnation temperature when the heat loss rate is equal to the heat absorbed, $G\tau\alpha - U_L(T_p - T_a) = 0$. A higher absorber plate temperature indicates a lower heat loss coefficient, U_L, due to the absence of (or a significant decrease of) gas conduction. In this equation G is the insolation from the solar simulator (W/m²), τ is transmissivity, α is absorbance, T_p and T_a are the copper plate and ambient temperatures, respectively.

Comparing the temperatures on the top and bottom glass panes of the enclosure (Figure 3), the top pane temperature increased at a faster rate during the early heating phase. This is a result of the higher absorbance (0.19) of the low-e coated glass heated directly by radiation. The temperature of the top pane decreased at a faster rate than bottom pane during the cool down phase, this may be due to higher convective heat transfer coefficients on an upwards-facing heated surface compared to a downwards-facing surface. The lower heat transfer coefficient at the bottom pane leads to a longer time constant and therefore remains hotter for longer.

Following the success of the enclosure tests described here, a water cooled absorber was built and assembled in an enclosure to create a complete evacuated flat plate solar thermal collector. This is the subject of a parallel investigation at the University of Warwick (Moss et al., 2018a; 2018b; 2018c; Moss et al., 2017).

3.6 Estimation of Absorbance, Emissivity and Gas Conductivity from the Transient Data

The transient testing enabled an estimation of the copper plate absorbance and allowed an investigation of the heat transfer from the copper plate absorber to the surroundings. The copper absorber was painted with Solkote and the measured plate emissivity was $\varepsilon_p = 0.5$ and $\varepsilon_p = 0.64$ for the bottom and top surfaces respectively. As glass is opaque to long-wavelength infra-red the effective emissivity of the glass was taken as a nominal, $\varepsilon_g = 0.96$, rather than the 0.16 which is typical for hard low emissivity coatings. The radiative heat transfer between two infinite parallel plates is given by $\dot{q}_{12} = \varepsilon_{pg}\sigma(T_1^4 - T_2^4)$ where the effective emissivity is $\varepsilon_{pg} = \left(\frac{1}{\varepsilon_p} + \frac{1}{\varepsilon_g} - 1\right)^{-1}$. The combination of Solkote and glass emissivities implies a combined emissivity of $\varepsilon_{pg} = 0.49$ and $\varepsilon_{pg} = 0.623$ for bottom and top surfaces respectively.

A one-dimensional transient heat balance analysis, including both radiative and conductive heat losses, can be modelled by equation (1), where T_p is the plate (absorber) absolute temperature, w is the copper area density (kg/m^2), c is the plate specific heat capacity and T_{g1} and T_{g2} are the top and bottom glass temperatures, respectively.

$$(wc)_p \frac{dT_p}{dt} = G(\tau\alpha) - \varepsilon_{pg}\sigma\left(T_p^4 - T_{g1}^4\right) - \varepsilon_{pg}\sigma\left(T_p^4 - T_{g2}^4\right) - h_1\left(T_p - T_{g1}\right) - h_2(T_p - T_{g2})$$
$$= G(\tau\alpha) - 2\varepsilon_{pg}\sigma\, T_p^4 + \varepsilon_{pg}\sigma\, T_{g1}^4 + \varepsilon_{pg}\sigma\, T_{g2}^4 - (h_1 + h_2)T_p + h_1\, T_{g1} + h_2 T_{g2} \qquad (1)$$

σ is the Stefan-Boltzmann constant, h_1 and h_2 are the heat transfer coefficients for the top and bottom glass panes respectively. This equation models the transient heating effect of the copper plate due to the illumination and includes heat losses between the copper plate and the inwards-facing surfaces of the glass panes. The net heat flux $(wc)_p \frac{dT_p}{dt}$ (shown in Figure 5) is obtained by numerical differentiation of the plate temperature data. The $(\tau\alpha)$ product is a function of glass transmittance and the Solkote absorbance at solar wavelengths. In terms of discrete parameters, the radiation absorbed by the plate is the sum of the direct illumination and any radiation that is reflected back by the glass i.e. $(\tau\alpha)_{overall} = \frac{\tau_e \alpha}{1-(\rho_e(1-\alpha))}$, α is the absorbance of the Solkote. The nominal overall values of transmittance and reflectance for a 4mm pane of low-e glass are $\tau_e = 0.71$, $\rho_e = 0.1$, respectively.
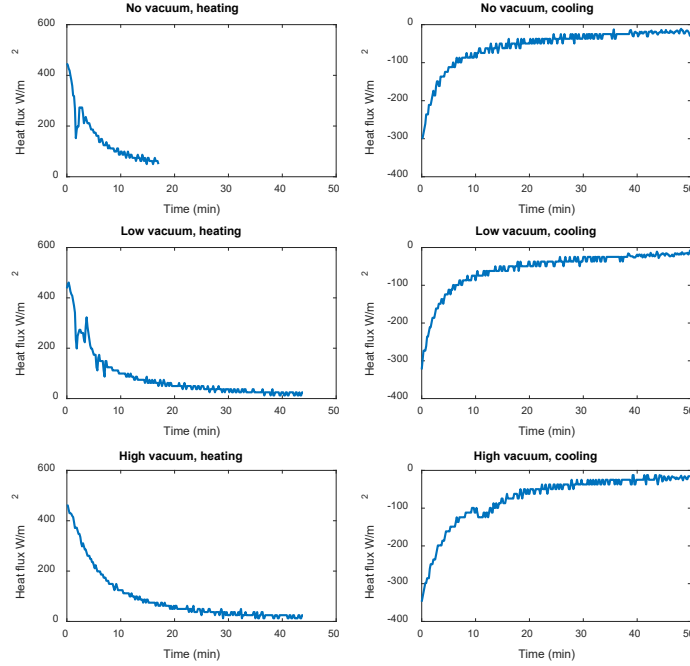

Figure 5. Heat fluxes to be achieved by the curve fitting.

The irregularities apparent on Figure 5 are thought to be due to instrumentation or interference effects. The deviation from a constant smooth curve is responsible, in part, for the wide confidence limits presented in Table 2.

The purpose of the analysis is to infer values of ε_{pg}, $G(\tau\alpha)$ and h from the absorber temperature curves and compare them with theoretical levels. A simple, single degree of freedom model was used taking the measured glass temperatures as input parameters.

The gap between the absorber plate and top glass is 6.3 mm and the absorber and bottom glass is 8mm. Assuming that the heat transfer coefficients due to conduction obey a conduction law, $h = \frac{k}{d}$, as a result the conduction terms in equation (2) can be merged:

$$(wc)_p \frac{dT_p}{dt} = G(\tau\alpha) - 2\varepsilon_{pg}\sigma\, T_p^4 + \varepsilon_{pg}\sigma\, T_{g1}^4 + \varepsilon_{pg}\sigma\, T_{g2}^4 - k(d_1^{-1} + d_2^{-1})T_p + kd_1^{-1}T_{g1} + kd_2^{-1}T_{g2} \qquad (2)$$

Where k is the conductivity and d is the distance between the glass pane and the absorber. Under high vacuum conditions (0.0033 Pa) the gaseous conduction should approximate zero, however heat transfer through the glass blocks supporting the copper absorber plate which act as thermal bridges will exist. Analysing the plate and glass temperatures, this heat transfer is unlikely to be distinguishable from the gas conduction. An attempt was made to generate a least-squares fit to the data, equation (3):

$$(wc)_p \frac{dT_p}{dt} = p_1 + p_2 \left(-2\sigma\left(T_p^4 - T_g^4\right)\right) + p_3\left(-T_p(d_1^{-1} + d_2^{-1}) + T_{g1}d_1^{-1} + T_{g2}d_2^{-1}\right) \tag{3}$$

Where p_1, p_2, p_3 are best-fit estimates for $G\tau\alpha, \varepsilon$ and k. The curve-fitting was performed for the heating period of each test and separately for the cool-down period. To assess the accuracy of the fit, equation (3) was solved numerically using the ODE23 function in MATLAB to predict the plate temperature history, as shown in Figure 6, using the fit parameters p_1, p_2, p_3 and the experimental T_g curves.
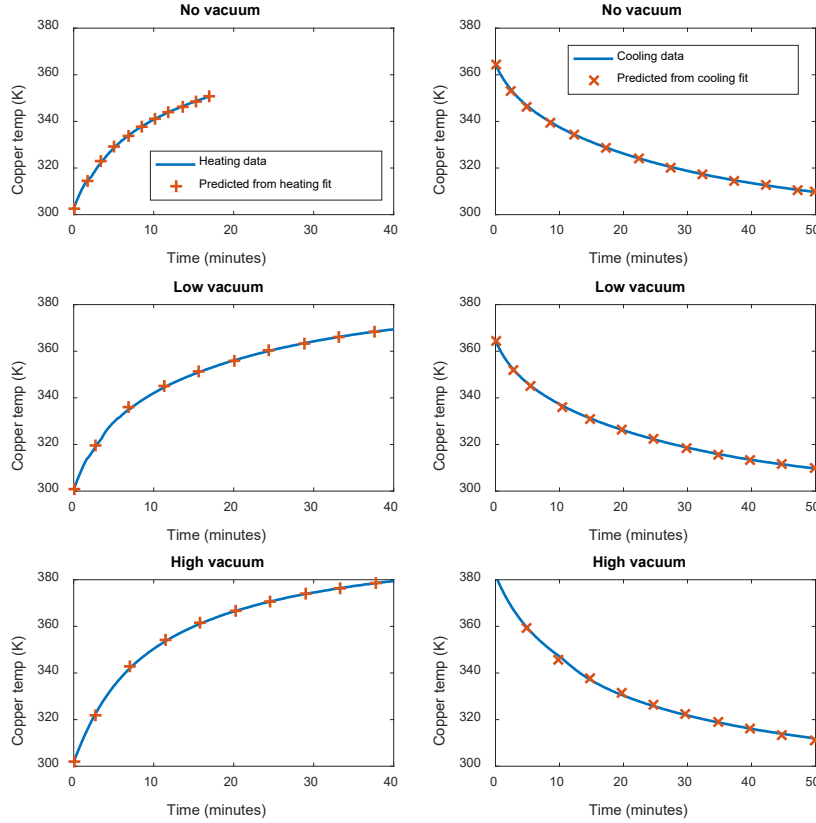

Figure 6. Simulated copper plate temperature history based on curve fit coefficients from the heating and cooling data.

The fit parameters are summarised in Table 2. The curve fits are in close agreement to the experimentally derived data but the variation in the curve-fit values of emissivity and heat transfer coefficient between the heating and cooling tests, and the use of negative values to achieve the best fit in some instances, suggests that the model requires further refinements.

Table 2. Least-squares fitting parameters for rate of copper absorber plate temperature change as a function of plate and glass temperature, equation (2).

	Parameter	No vacuum, $G = 797$ W/m²		Low vacuum, $G = 777$ W/m²		High vacuum, $G = 769$ W/m²	
		coefficient	limits	coefficient	limits	coefficient	limits
Heating	P_1 ($G\tau\alpha$)	459.0	[434.0, 485.0]	474.0	[462.0, 486.0]	510.0	[505.0, 515.0]
	$\tau\alpha$	0.623	[0.588, 0.657]	0.63	[0.614, 0.646]	0.709	[0.702, 0.717]
	P_2 (ε multiplier)	0.876	[0.413, 1.34]	0.915	[0.844, 1.0]	0.779	[0.755, 0.803]
	P_3 (k)	0.0214	[0.00436, 0.0384]	0.0172	[0.0131, 0.0205]	0.00953	[0.00833, 0.0107]
Cooling	P_1 ($G\tau\alpha$)	19.7	[15.1, 24.3]	12.9	[9.41, 16.3]	-13.7	[-16.8, -10.6]
	P_2 (ε multiplier)	-2.03	[-2.65, -1.4]	-1.35	[-1.84, -0.871]	-0.0104	[-0.266, 0.245]
	P_3 (k)	0.151	[0.126, 0.176]	0.118	[0.0988, 0.138]	0.0351	[0.0243, 0.0458]

The 95% confidence limits for the coefficients shows considerable variability in the degree to which the data matches equation (2). The confidence limits are provided by MATLAB's curve-fitting toolbox and are a statistical measure of the certainty in determining each coefficient given the standard deviation of the data values relative to the best fit curve. The high vacuum heating test has the closest tolerance on p1 and p2; other heating tests i.e. low vacuum and no vacuum tests have close tolerances on p3. The cooling tests exhibit wide tolerances on all coefficients: negative values are unrealistic in practice and the p1 value is expected to be zero.

The predicted air conductivity values from the heating test at atmospheric pressure, 0.0214 W/mK, are lower than expected; a typical dry air conductivity of 0.0285 W/mK at 60°C would however lie within the confidence limits. The decrease in conductivity from atmospheric to low vacuum (0.0214 to 0.0172) may indicate that convection has been inhibited (Eaton and Blum, 1975). The large decrease in conductivity to 0.00548 in the high vacuum test would indicate that the vacuum has significantly reduced the heat loss due to conduction. There will remain some heat transfer by conduction in the residual gas and the plate support blocks.

The emissivity multipliers in the range of 0.833 to 0.915 for the heating tests suggest that the combined emissivity for the copper plate and glass is lower than the expected ε_{pg} values (0.49 bottom side, 0.623 top side) based on spot measurements using an emissometer. This is most likely due to the thermocouples recording a spot temperature measurement rather than a mean glass temperature.

The curve fit parameters for the cooling tests differ significantly from the heating test equivalents and have wide confidence limits; this was unexpected. The negative values are highly unrealistic while the non-zero values for $G\tau\alpha$ are also unrealistic in the absence of illumination. The glass temperatures are sensibly uniform during the early part of the heating experiments since they start from a uniform (ambient) temperature. The copper plate temperature, which is assumed to be uniform due to the high conductivity of copper, can then be modelled well in terms of heat transfer based on the glass temperature.

As each test progresses the thermocouple temperature values asymptote towards a steady state limit. There must also be a trend towards a steady-state temperature profile across the top and bottom glass panes due to the variation in natural conductive heat transfer coefficients over the surface (Sparrow and Carlson, 1986; Yu and Lin, 1993). At the start of the cooling tests (after 2-5 hours heating), the glass temperature would have been highly non-uniform. The growth of the thermal boundary layer as the air moves over the surface would result in the top surface being hotter in the centre and the bottom surface being hotter towards the edge. The upwards-facing and downwards-facing heat transfer coefficients have very different distributions so the effects of these do not counteract each other. In addition, the thermocouples on the glass panes may not give an accurate indication of the mean surface temperatures during the cooling test, resulting in curve fit coefficients that appear unrealistic.

A further more general source of error is that radiative and conductive heat fluxes are both approximately proportional to $(T_p - T_g)$:

Conduction: $\dot{q}_{cond} = \frac{k}{d}(T_p - T_g)$

Radiation: $\dot{q}_{rad} = \varepsilon_{pg}\sigma(T_p^4 - T_g^4) = \varepsilon_{pg}\sigma(T_p - T_g)(T_p + T_g)(T_p^2 + T_g^2)$

The majority of the captured data covers a small range in $(T_p + T_g)(T_p^2 + T_g^2)$ as shown in Figure 7. Both coefficients p2 and p3 have very similar effects on the heat flux and it is difficult to distinguish between them. The presence of any random noise in the data or any deviation from the proposed formula in equation (3), will then introduce considerable uncertainty in the coefficients obtained.
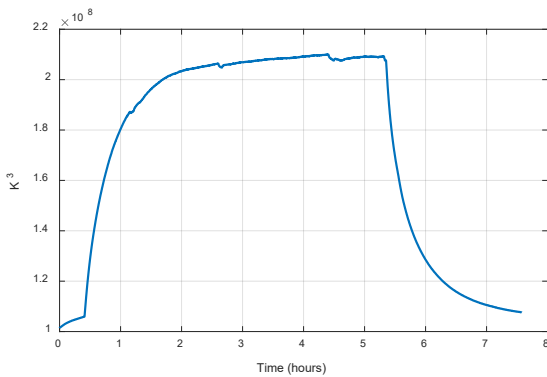

Figure 7. Variation in $(T_p + T_g)(T_p^2 + T_g^2)$ during the vacuum test.

The curve fit is highly sensitive to the variation in $(T_p - T_g)$ during a test. To investigate the sensitivity of the fit parameters to small changes in glass temperature, the curve fit for the low vacuum cooling test was repeated with increments in the range of $\pm 3\,K$ added to the glass temperatures as shown in Figure 8. A decrease in glass temperature of 2.77 °C was found to bring the coating emissivity and gas conductivity close to the expected values (Figure 8b, 8c) but the curve fit then requires $G\tau\alpha \approx 35\,W/m^2$. Conversely, an increase of 0.52°C would achieve the desired un-illuminated $G\tau\alpha \approx 0\,W/m^2$ (Figure 8a) but with implausible values (negative ε, conductivity of 3× higher than expected) for the other two coefficients. Given that the glass temperatures increased by 45°C during the heating phase a considerable temperature non-uniformity might be expected across the enclosure. It is possible that the mean value could differ significantly from the thermocouple readings and that curve fitting using a non-uniform temperature distribution (if known) might achieve a better balance of the coefficients.
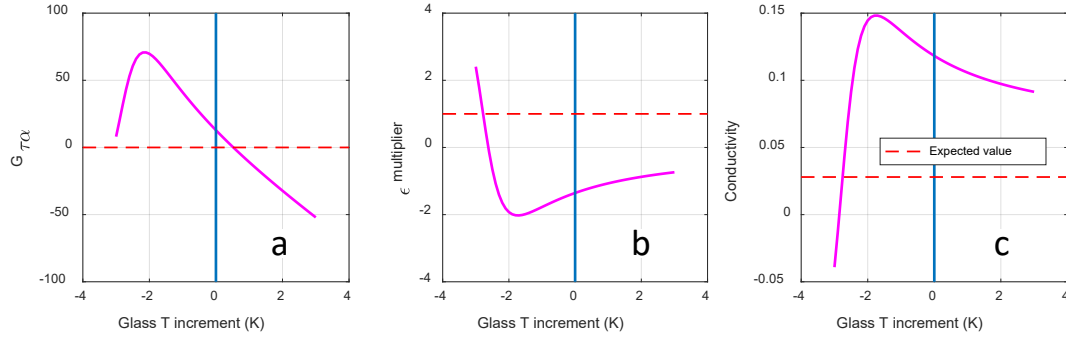

Figure 8. Sensitivity of curve fit parameters to an offset in glass temperatures.

The fact that a constant adjustment to temperatures during the cooling test fails to give acceptable values for all three parameters may be an indication that the temperature distribution (and therefore the difference between mean and thermocouple temperature) changes as the enclosure temperature decreases. Future investigations will investigate the use of a fan to raise the external heat transfer coefficient above that of natural convection. This will cool the glass so it remains closer to ambient temperature, hence more uniform, thereby avoiding this uncertainty.

Figure 9 compares the predicted low vacuum plate cooling history with these two adjustments together with a simulation using the heating test coefficients (ε multiplier 0.915, k=0.0172) with zero irradiance, $G\tau\alpha \approx 0$.
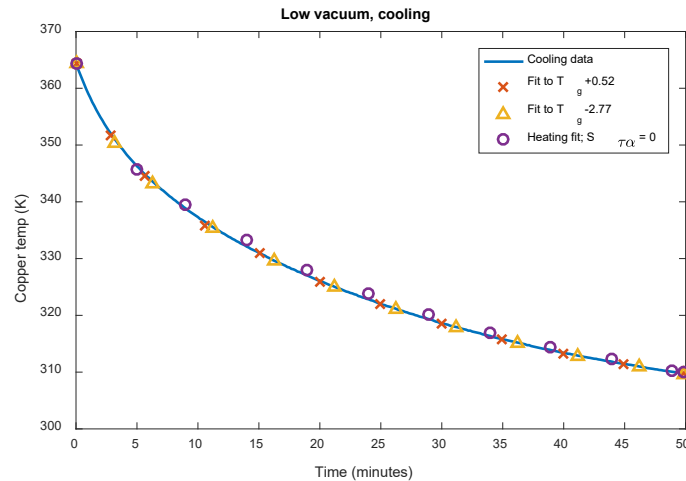

Figure 9. Low vacuum cooling test: comparison of copper plate temperature data with three simulations using different coefficients.

As the three predictions are close to the data curve it is suggested the curve fit method is unable to distinguish between the four parameters ($G\tau\alpha$, ε, k and a temperature error). Given that the glass temperatures are expected to be non-uniform and that this is not included in the modelling the curve fit

process is not expected to yield exact values. Its merit is simply to illustrate trends in heat loss while the pressure is reduced and to aid interpretation of the experimental results.

3.7 Prediction of Steady State Performance

The enclosure and copper plate are modelled as if the plate were water-cooled and could be maintained at any arbitrary temperature T_p. At steady state conditions, the temperature of each glass pane will be such that the net heat flux into the glass is zero:

$$[\varepsilon_{pg,j}\sigma(T_p^4 - T_{g,j}^4) + h_{j,int}(T_p - T_{g,j}) + \dot{q}_{abs,glass}] - [\varepsilon_{gs,j}\sigma(T_{g,j}^4 - T_a^4) + h_{j,ext}(T_{g,j} - T_a)] = 0, \quad j = 1, 2$$

- $h_{j,int}$ is the heat transfer coefficient between the glass and copper plate, and $h_{j,ext}$ is the heat transfer coefficient between the glass and the surrounding ambient environment.
- $\dot{q}_{abs,glass}$ is the rate of heat absorption in the glass due to the light passing through it. For low iron glass this would be close to zero but in low emissivity glass the absorbance can be as high as 0.19 which would lead to significant heat absorption.
- T_a, T_g and T_p are absolute temperatures (K) of the ambient environment, each glass pane (j = 1,2) and the absorber plate.

The internal heat flux from the absorber plate to glass (plus any radiation absorbed in the glass) must equal the external heat loss from the glass to the surroundings. This fourth order equation can be solved in MATLAB to determine the temperatures of the top glass $T_{g,1}$ and bottom glass $T_{g,2}$, using values for heat transfer coefficients based on natural convection correlations and the measured emissivities. This technique differs from the approach used by Akhtar and Mullick (2007) who proposed empirical correlations for the glass temperature.

The long wavelength radiative heat fluxes do not include any terms for transmission through the glass as it is opaque at long wavelengths (>2500nm). For strict accuracy infinite geometric series are summed to include the absorbance of light after multiple reflections from the copper plate:

$$\dot{q}_{abs,\ glass} = G\alpha_g\left(1 + \frac{\tau_g\rho_p}{1 - \rho_p\rho_g}\right), \text{ taking } \alpha_g = 0.19, \ \rho_g = 0.1, \ \tau_g = 0.71 \text{ for 4 mm low emissivity glass at}$$

solar wavelengths. The plate reflectivity is $\rho_p = 1 - \alpha_p$.

When steady-state glass temperatures have been determined the net heat flux to the plate is calculated:

$$\dot{q}_{plate} = G\left(\frac{\tau_g\alpha_p}{1 - \rho_p\rho_g}\right) - \sum_{j=1,2}[\varepsilon_{pg,j}\sigma(T_p^4 - T_{g,j}^4) + h_{j,int}(T_p - T_{g,j})]$$

Solkote has an absorptivity (α_p) of 0.913; this implies $(\tau\alpha)_{overall} = 0.654$ which is consistent with the mean of the three heating test curve fits in Table 2, and is in the middle of the specified absorptivity range. The internal conduction and convection heat transfer coefficient between the copper absorber plate and glass was based on a correlation by Hollands et al. (1976):

$$Nu = 1 + 1.44\left[1 - \frac{1708(sin1.8\beta)^{1.6}}{Ra\ cos\beta}\right]\left[1 - \frac{1708}{Ra\ cos\beta}\right]^+ + \left[\left(\frac{Ra\ cos\beta}{5830}\right)^{\frac{1}{3}} - 1\right]^+$$

coupled with a reduction in conductivity at very low pressures as described in Part 1 of this paper.

For radiation between the glass and surroundings it was assumed that any surfaces exchanging radiation with the enclosure were at ambient temperature. The laboratory walls, floor and ceiling represent a much larger area than the enclosure and were therefore treated as a black body. The effective emissivity is then equal to the glass emissivity: $\varepsilon_{gs,1} = \varepsilon_{gs,2} = \varepsilon_g = 0.16$ for the low emissivity surface of the glass pane. Regardless of the wall emissivity, very little of the thermal radiation emitted by the glass is likely to be reflected off the walls and back onto the glass (Gray and Müller, 1974). The simulator in this study included a "cold sky" IR filter to eliminate long wavelength radiation due to the temperature of the lamp assembly.

The external heat transfer coefficient was calculated from natural convection correlations (ASHRAE, 2009, as collated by Jaffer, 2011) for a horizontal plate:

- Hot side facing upwards $Nu = (0.65 + 0.36Ra^{1/6})^2$

- Hot side facing downwards $Nu = \dfrac{0.544 Ra^{0.2}}{\sqrt[3]{1+\left(\frac{0.785}{Pr}\right)^{0.6}}}$

Pr is Prandtl number, Nu is Nusselt number and Ra is Rayleigh number. Conductivity was evaluated at the glass temperature but other fluid properties were calculated at a film temperature. The characteristic length for the non-dimensional groups is $L = \dfrac{WH}{2(W+H)} = \dfrac{area}{perimeter}$.

The resulting heat transfer coefficient $h_{j,ext}$ varies with the glass temperature so an iterative procedure was used; 5 iterations were sufficient to reach a stable solution.

Simulations undertaken at higher plate temperatures show increased heat losses and reduced efficiency as a solar collector, Figure 10(a). The zero-efficiency intercept models the experimental case where the plate is in thermal equilibrium with the enclosure i.e. $\dot{q}_{plate} = 0$. Figure 10(b) presents the calculated overall heat loss coefficients for each condition using the equation below:

$$U_L = \frac{\sum_{j=1,2}\left[\varepsilon_{pg,j}\sigma\left(T_p^4 - T_{g,j}^4\right) + h_{j,int}\left(T_p - T_{g,j}\right)\right]}{T_p - T_a}$$

The increase in heat loss coefficient with temperature, Figure 10(b), shows the effects of increasing natural convection Nusselt numbers and radiative losses as the glass temperature increases at high copper plate temperatures.
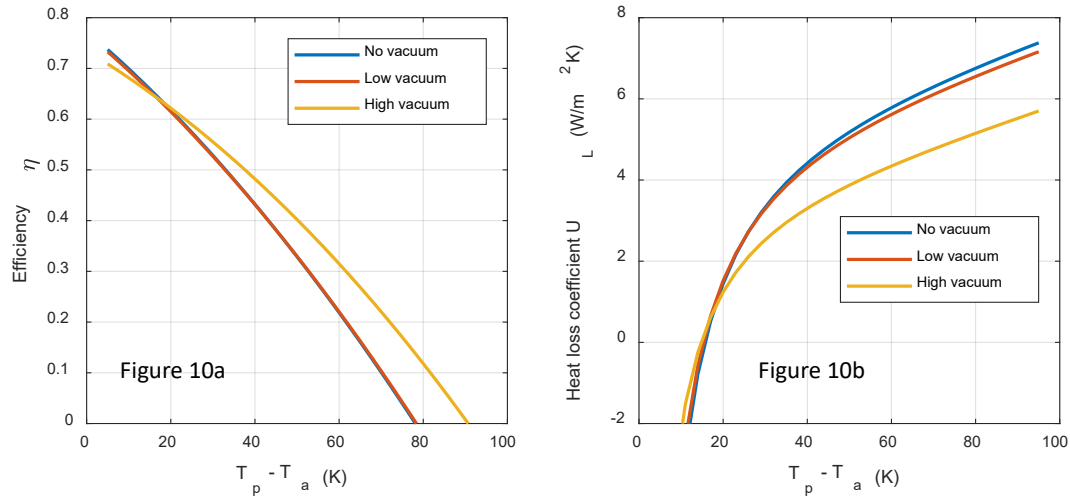

Figure 10. Predictions of (a) steady-state efficiency and (b) copper plate heat loss coefficient.

The high vacuum scenario generally has higher efficiency levels and a lower heat loss coefficient than the low vacuum and atmospheric tests. Figure 10(b) shows a negative copper plate heat loss coefficient when $T_p - T_a < 16°C$ as the top glass is then hotter than the copper absorber plate due to absorption of the incident radiation; there is some heat transfer from glass to plate. The conduction of heat from glass to plate is more pronounced in the low and no vacuum cases, hence exhibiting higher predicted efficiencies than the high vacuum case when operating at $T_p - T_a < 16°C$. This unusual situation is due to the high absorbance of the low emissivity glass; with high transparency glass and a solar spectrum, only a small fraction of the incident radiation would be absorbed in the glass and its temperature (for low T_p) would remain close to ambient. The adiabatic plate temperatures are in excellent agreement with the asymptotic values from the heating tests (Table 1). This gives confidence when using the model to aid interpretation of the transient results.

3.8 Time Constants for Absorber and Enclosure

When interpreting the transient temperature data the collector may be considered to be a system of components with first-order time constants (exponential decay). Pierson and Padet (1990) and Wijeysundera (1978), have developed more detailed transient analytical models for solar collectors; these however apply to absorbers with a cooling flow rather than an isolated plate.

For simplicity, the analysis shall consider this as a linearised single degree of freedom first order system in which a flat plate initially at temperature T_0 responds to a step change in conditions such as illumination

from a solar simulator. The plate exchanges heat with another surface or the environment at constant temperature T_0 in accordance with a heat transfer coefficient h. The plate, with area density of w and specific heat capacity of c, absorbs $\dot{q}$ (W/m^2) of light (energy) from the simulator; its instantaneous temperature is T where $wc\frac{dT}{dt} + hT = \dot{q} + hT_0$. The solution is $T = T_0 + \frac{\dot{q}}{h}\left[1 - e^{-\frac{h}{wc}t}\right]$ and has a time constant of $\frac{wc}{h}$.

During a transient test the glass and copper plate temperatures will vary along with the heat transfer coefficients (as indicated by Fig 10(b)). The results from the steady-state simulation give an indication of typical heat transfer coefficients and their variation with plate temperature as illustrated in Figure 11. The plate is held at temperature T_p and the glass is in equilibrium with the plate temperature. These results were used to inform the choice of nominal heat transfer coefficients for theoretical estimation of glass and plate time constants.
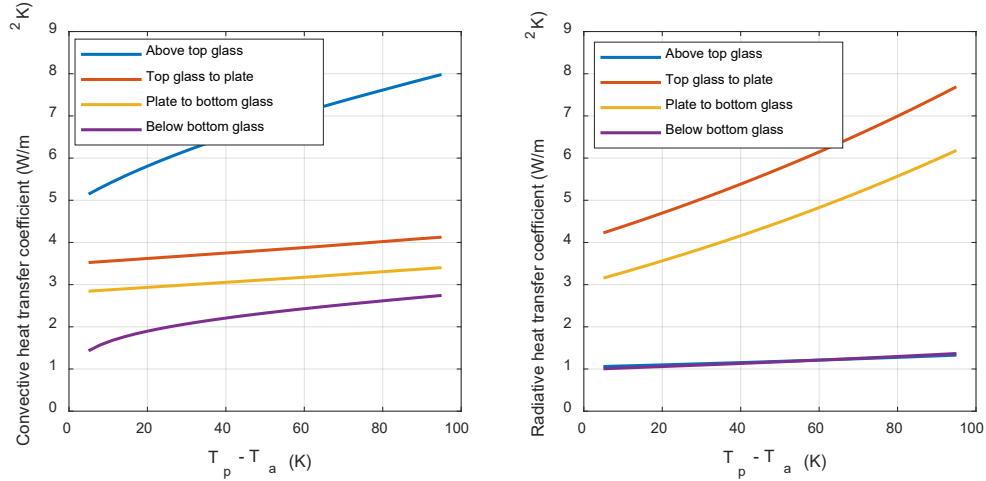

Figure 11. Steady state predictions of heat transfer coefficients for a conceptual enclosure at low vacuum.

Heat transfer coefficients for components at typical mean conditions from the low and high vacuum steady state predictions over the warm-up period (low vacuum, mean over first 40 minutes: $T_p - T_a = 52.2°C$; high vacuum, mean over first 60 minutes: $T_p - T_a = 68.4°C$) are presented in Table 3.

Table 3. Heat transfer coefficients for components.

		Convection or conduction, upwards	Radiation upwards	Convection or conduction, downwards	Radiation downwards	Total (W/m²K)
Low vacuum	Top glass	6.87	1.19	3.83	5.84	17.7
	Plate	3.83	5.84	3.13	4.56	17.4
	Bottom glass	3.13	4.56	2.35	1.18	11.2
	Whole system	6.87	1.19	2.35	1.18	11.6
High vacuum	Top glass	7.04	1.21	0.00422	6.36	14.6
	Plate	0.00422	6.36	0.00421	4.98	11.3
	Bottom glass	0.00421	4.98	2.41	1.2	8.6
	Whole system	7.04	1.21	2.41	1.2	11.9

The "whole system" values are higher than the overall heat loss coefficient U_L because the latter is based on the difference in copper plate temperature to ambient temperature $T_p - T_a$ whereas the other coefficients are calculated in terms of a smaller temperature difference as $T_g - T_a$. The total heat transfer coefficients from Table 3 and material properties are used to calculate time constants, as shown in Table 4. The glass panes have a significantly longer time constant than the copper plate.

Table 4. Heat transfer coefficients, thermal capacitance and predicted time constants for the components (high vacuum).

Material	h (W/m²K)	wc (KJ/m²K)	Time constant (min)
Top glass + pillars (half)	14.6	10.05	11.5
Copper	11.3	3.06	4.5
Bottom glass + pillars (half)	8.6	10.05	19.5
Whole system	11.9	23.17	32.6

The short time constant for the copper plate is a consequence of it rapidly reaching equilibrium with the glass temperature. The longer glass time constant slows the response of the whole system, with the glass gradually approaching its steady state condition. The overall time constant is governed by the external heat transfer coefficients resulting in cool-down times for the three tests which are broadly similar (Table 3). The time response of the temperature difference between the copper plate and top glass is presented in Figure 12. The copper plate temperature rapidly approaches a quasi-equilibrium state with the glass temperature; the glass temperature rises more slowly (longer time constant). During this warm-up period the heat flux from plate to glass is lower than the steady state value: hence the plate temperature increases.
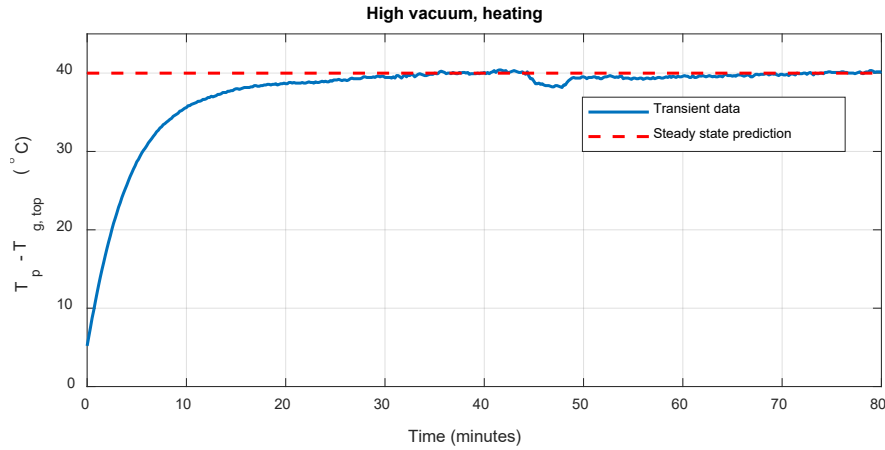

Figure 12. Time response of the temperature difference between the copper plate and top glass.

Figure 13 compares the transient glass temperature data with a series of steady state (equilibrium) predictions based on instantaneous plate temperature. The data curves show the transient response relationship between the glass and plate temperatures; the equilibrium lines indicate the glass temperatures that would be expected over a range of illumination levels corresponding to steady state $T_p - T_a$ values on the x-axis.
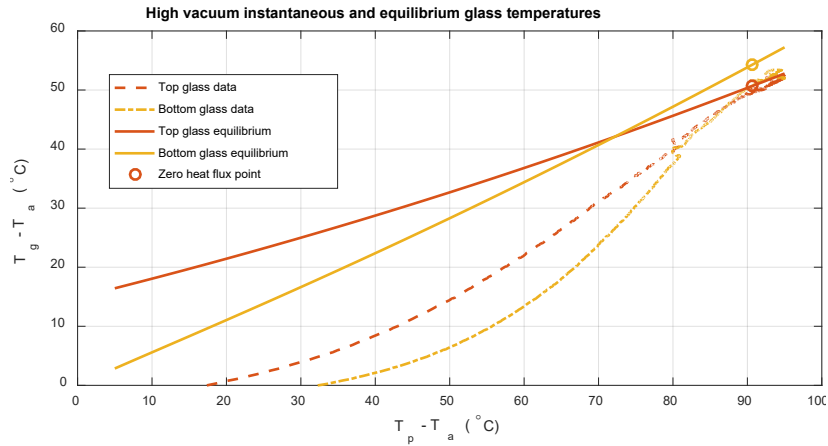

Figure 13. Comparison of transient glass temperature data with steady state prediction (equilibrium) at the same copper plate temperature.

At any given plate temperature during the warm-up period the glass temperature is lower than the equilibrium temperature. This would be expected in most transient heating tests. However if the glass time constant was shorter than the plate time constant, the glass temperatures would be closer to the steady state line. It must be remembered that the thermocouples measure a point temperature, near the centre of the surface, whereas the prediction assumes the whole surface is at uniform temperature.

When $T_p - T_a < 70°C$ the top glass pane is predicted to be hotter than the bottom glass pane because it absorbs part of the radiation; there is also increased radiative heat transfer from the copper plate to glass as the top surface of the copper plate has a higher emissivity. The top surface of the enclosure however has a

higher convective heat transfer coefficient than the underneath as it produces a strong plume of hot air rising off the plate; conversely the downwards-facing surface of the enclosure generates a much weaker plume where air heated by conduction escapes laterally and is replaced by cooler air from below, leading to lower Nusselt numbers. This mechanism is modelled by the standard Nusselt-Grashof number correlations for horizontal flat plates. The test passes through this transient phase, due to the high illumination level, before reaching higher copper plate temperatures; From this point on, $T_p - T_a > 70°C$ and the steady-state prediction is for the bottom glass to be hotter than the top due to the increasing difference between upper and lower surface convective heat transfer coefficients.

The higher heat transfer coefficient on the top pane surface results in the shallower gradient as shown in Figure 13 and when $T_p - T_a > 70°C$ a lower temperature is predicted for the top surface compared to the bottom surface. Under equilibrium conditions (shown as zero net heat flux in Figure 13) the top glass pane of the enclosure is predicted to be 3.6°C cooler than the bottom glass pane for the test condition $G = 770$ W/m². A test under lower radiation levels might conversely be able to reach equilibrium with the top glass hotter than the bottom glass.

In practice the two convective flow regimes produce varying distributions of thermal boundary layer thickness and heat transfer coefficient over the surfaces. The bottom surface will experience a peak heat transfer coefficient in the centre of the enclosure where the boundary layer is thinnest; conversely the top surface will have the highest heat transfer coefficients around the edge of the enclosure. This effect is visible at the zero heat flux points in Figure 13 for the bottom glass; the top glass thermocouple temperatures however agree well with the predictions and show no evidence of a temperature profile across the glass.

Figure 14 illustrates exponential decay curve fits to the copper plate and glass temperatures. The second order fit to the copper plate temperature is given by:

$$T_p - T_a = 52.75\left(1 - e^{-\frac{t}{6.69}}\right) + 37.83\left(1 - e^{-\frac{t}{37.8}}\right) + 2.46$$

The copper plate response is the sum of two components i.e. first-order and second-order fit with time constants of 6.69 and 37.8 minutes respectively. The 37.8 minute constant (Table 5) is close to the 32.6 minute predicted time constant for the whole system (Table 4). The short time constant (6.69 minutes) is closer to the 4.5 minute predicted plate time constant for the high-vacuum test. The time constant for the top glass (24.1 minutes) is between the expected values for the whole system (32.6 minutes) and top glass (11.5 minutes). Similarly the time constant for the bottom glass (27.3 minutes) is between the expected values for the whole system (32.6 minutes) and bottom glass (19.5 minutes).
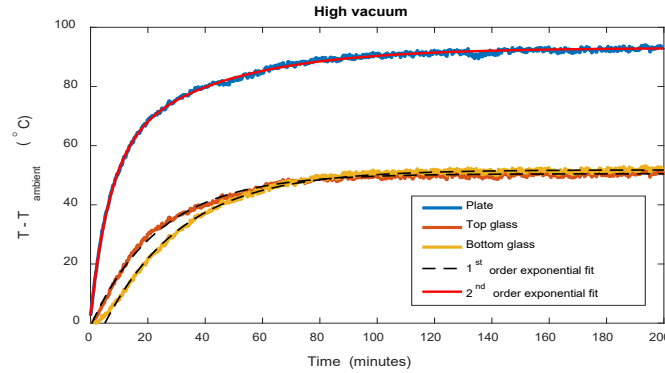

Figure 14. Exponential decay curve fits to the copper plate and glass temperatures.

Table 5. First order curve fit coefficients for high vacuum heating data (Figure 14).

	Predicted steady state $T - T_a$ (°C)	Experimental $T - T_a$ asymptote (°C)	First curve fit time constant (minutes)	Second time constant
Top glass	42.4	50.5	24.1	
Copper Plate	90.1	93	6.69	37.8
Bottom glass	53.9	51.8	27.3	

3.9 Unsteady Heat Balance Simulations

The steady-state simulation was modified to return instantaneous heat fluxes for any combination of ambient, copper plate and glass temperatures and an Euler integration algorithm was used with 10 second time steps to predict the temperature traces given by equation (6), as shown in Figure 15.

$$T_{i+1,j} = T_{i,j} + \frac{dT_{i,j}}{dt}\Delta t, \qquad \frac{dT_{i,j}}{dt} = \frac{\dot{q}_{i,j}}{(wc)_i}, \qquad j = 1:3, \quad i = 1:600 \qquad (6)$$
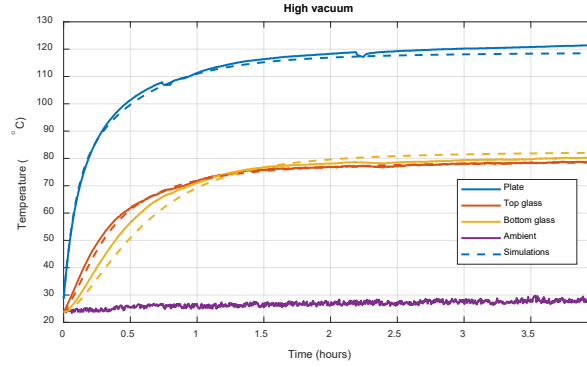

Figure 15. Transient simulation of copper plate and glass temperatures for the high vacuum heating test.

The simulation agrees well with the experimentally measured results though during the first hour of heating the predicted temperatures for the bottom glass pane are a few degrees below the experimental measurements. This could result from non-uniformity in the Solkote emissivity over the underside of the plate. As in the steady state predictions, both the bottom glass and the copper plate asymptote to temperatures higher than the experimentally measured values, however the overall agreement is good. Evacuated solar collector performance can therefore be predicted accurately using generic heat transfer correlations.

4. Conclusions

Two flat vacuum enclosures were fabricated using low emissivity glass and a stainless steel edge spacer. One enclosure (Part 1 paper) was empty with the low-emittance coatings facing the cavity while the other enclosure had low emittance coatings facing the external environment and contained a copper absorber plate (Part 2 paper). The enclosure with an integrated copper plate was tested under a solar simulator as if it were a solar thermal collector. Under high vacuum (0.0033 Pa), low vacuum (17 Pa) and no vacuum conditions in the enclosure, the absorber reached temperatures of 122.8°C, 104.2°C and 103.6°C, respectively. The high vacuum conditions reduced the heat loss coefficient demonstrating the potential for improved performance in a complete solar collector with a water-cooled absorber.

A prediction of copper plate temperature based on measured glass temperatures and curve fit parameters to a three-term heat flux model is in excellent agreement with experimentally measured data; the fit parameters for the heating tests are close to expected values for absorbance, emissivity and conductivity. Coefficients derived from the cooling tests are more variable. A possible explanation is that after prolonged heating a temperature profile has developed across the glass panes and the thermocouples give spot temperatures rather than an accurate measure of the mean glass temperatures.

A steady state prediction for the complete enclosure solved the heat balance equation; the predicted copper plate temperature was in close arrangement with the experimental steady-state temperatures over all three tests. The measured top glass pane temperature corresponded with the predictions, however the measured bottom glass temperature, near the centre of the pane, was lower than the predictions. This is due to the free convection heat transfer coefficient being higher at this position than the surface mean value.

The transient response of the copper plate and glass may be qualitatively explained by a single degree of freedom lumped model. The copper plate (0.9 mm thick) had a shorter time constant than the collector system as a whole. The time constants for the glass panes were found to lie between the predicted time constant for a single 4 mm glass pane and that for the whole system. The transient predictions agreed well with the measured copper plate and top glass temperatures, indicating that the correlations used are applicable over a wide temperature range.

The thermal performance of an evacuated enclosure can be accurately predicted using a simple heat transfer equation. The correlations used in the prediction are appropriate for this application.

It can be concluded that the vacuum enclosure provides excellent thermal insulation around the test absorber plate. Replacing the copper plate by a water-cooled absorber with a commercial low emissivity coating and utilizing low iron glass (i.e. very low absorbance), the efficiency under high vacuum would have exceeded conventional flat panel solar collectors. Evacuated flat plate solar collectors therefore have the potential to provide exceptional performance over a wide range of conditions and can be integrated into building skins as thermal insulation panels.

16

5. Acknowledgements

6. References

Akhtar, N., Mullick, S.C., 2007. Computation of glass-cover temperatures and top heat loss coefficient of flat-plate solar collectors with double glazing. Energy 32, 1067-1074.

Amer, E.H., Nayak, J.K., 1999. Evaluation of a transient test procedure for solar flat-plate collectors. Energy 24, 975-995.

Amer, E.H., Nayak, J.K., Sharma, G.K., 1997. Transient test methods for flat-plate collectors: review and experimental methods. Solar Energy Vol. 60 No. 5, 229-243.

Araldite data sheet, 2011. Available online at: https://polyestershoppen.nl/download/araldite-rapid-epoxylijm/araldite-rapid-datasheet-145.pdf

Arya, F., 2014. Developing alternative sealing materials in fabrication of evacuated glazing at low temperature. Thesis (PhD). Ulster University. http://ethos.bl.uk/OrderDetails.do?uin=uk.bl.ethos.629079

ASHRAE, 2009. ASHRAE Fundamentals Handbook (SI), American Society of Heating Refrigerating and Air-conditioning Engineers Inc., 2009, ISBN 978-1-931862-71-4.

Duffie, J.A., Beckman, A., 1991. Solar Engineering of Thermal Processes, Second edition, Wiley, 1991.

Eaton, C.B., Blum, H.a., 1975. The use of moderate vacuum environments as a means of increasing the collection efficiencies and operating temperatures of flat-plate solar collectors. Solar Energy 17, 151–158. http://dx.doi.org/10.1016/0038-092X(75)90053-5

Gray, W.A., Müller, R., 1974. Engineering calculations in radiative heat transfer, Pergamon Press, 1974. http://proceedings.ises.org/paper/eurosun2014/eurosun2014-0039-Moss.pdf

Hollands K., Unny T. Raithby G, and Konicek L., 1976, Free convective Heat Transfer Across Inclined Air Layers, Trans. of ASME : Journal of Heat Transfer vol. 190, pp. 189-193.

Jaffer, A., Online documentation for SimRoof, 2011. http://people.csail.mit.edu/jaffer/SimRoof/Convection/#Horizontal%20Plate.

Pierson, P., Padet, J., 1990. Time constant of solar collectors. Solar Enery Vol. 44 No. 2, 109-114.

Pugsley, A., Zacharopoulos, A., Smyth, M., Mondol, J., 2017. Performance evaluation of the senergy polycarbonate and asphalt carbon nanotube solar water heating collectors for building integration. Renewable Energy. Available online 28 October 2017. https://doi.org/10.1016/j.renene.2017.10.082.

R.W. Moss, G.S.F. Shire, P. Henshall, P.C. Eames, F. Arya, T. Hyde, 2018. Design and fabrication of a hydroformed absorber for an evacuated flat plate solar collector. Applied Thermal Engineering. Applied Thermal Engineering 138, 456–464

R.W. Moss, G.S.F. Shire, P. Henshall, P.C. Eames, F. Arya, T. Hyde, 2017. Optimal passage size for solar collector microchannel and tube-on-plate absorbers. Solar Energy 153, 718–731.

R.W. Moss, P. Henshall, F. Arya, G.S.F. Shire, P.C. Eames, T. Hyde, 2018. Simulator testing of evacuated flat plate solar collectors for industrial heat and building integration. Solar Energy 164, 109–118.

R.W. Moss, P. Henshall, F. Arya, G.S.F. Shire, T. Hyde, P.C. Eames, 2018. Performance and operational effectiveness of evacuated flat plate solar collectors compared with conventional thermal, PVT and PV panels. Applied Energy 216, 588–601.

Rodríguez-Hidalgo, M.C., Rodríguez-Aumente, P.A., Lecuona, A., Gutiérrez-Urueta, G.L., Ventas, R, 2011. Flat plate thermal solar collector efficiency: Transient behavior under working conditions. Part I: Model description and experimental validation. Applied Thermal Engineering 31, 2394-2404.

Rodríguez-Hidalgo, M.C., Rodríguez-Aumente, P.A., Lecuona, A., Gutiérrez-Urueta, G.L., Ventas, R, 2011. Flat plate thermal solar collector efficiency: Transient behavior under working conditions. Part II: Model application and design contributions. Applied Thermal Engineering 31, 2385-2393.

Sparrow, E.M., Carlson, C.K., 1986. Local and average natural convection Nusselt numbers for a uniformly heated, shrouded or unshrouded horizontal plate. Int. Journal of Heat and Mass Transfer 29(3) 369-379.

Wijeysundera, N.E., 1978. Comparison of transient heat transfer models for flat plate collectors. Solar Energy 21, Issue 6, 517-521.

Yu, W-S., Lin, H-T., 1993. Conjugate problems of conduction and free convection on vertical and horizontal flat plates. Int. Journal of Heat and Mass Transfer Vol. 36 No. 5 pp 1303-1313.